Revealing Fundamentals of Charge Extraction in Photovoltaic Devices Through Potentiostatic Photoluminescence Imaging

Lukas Wagner (lukas.wagner@ise.fraunhofer.de)
Fraunhofer ISE
Patrick Schygulla
Fraunhofer ISE https://orcid.org/0000-0001-9103-1045
Jan Herterich
Fraunhofer ISE
Mohamed Elshamy
Fraunhofer ISE
Dmitry Bogachuk
Salma Zouhair
Fraunhofer ISE https://orcid.org/0000-0002-1344-9101
Simone Mastroianni
Fraunhofer ISE
Uli Würfel
Fraunhofer ISE https://orcid.org/0000-0003-4151-8538
Yuhang Liu
École Polytechnique Fédérale de Lausanne
Shaik Zakeeruddin
Ecole Polytechnique Federale de Lausanne
Michael Graetzel
École Polytechnique Fédérale de Lausanne https://orcid.org/0000-0002-0068-0195
Andreas Hinsch
Fraunhofer Institute for Solar Energy Systems ISE
Stefan Glunz

Article

Keywords: photocurrent imaging, photoluminescence imaging, local analysis, short circuit current, charge extraction, perovskite solar cells, III-V solar cells

Posted Date: October 22nd, 2021

DOI: https://doi.org/10.21203/rs.3.rs-991022/v1

Abstract

The photocurrent density-voltage ($J(V)$) curve is the fundamental characteristic to assess opto-electronic devices, in particular solar cells. However, it only yields information on the performance integrated over the entire active device area. Here, a method to determine a spatially resolved photocurrent image by voltage-dependent photoluminescence microscopy is derived from basic principles. The opportunities and limitations of the approach are studied by the investigation of III-V and perovskite solar cells. This approach allows the real-time assessment of the microscopically resolved local $J(V)$ curve, the steady-state J_{sc}, as well as transient effects. In addition, the measurement contains information on local charge extraction and interfacial recombination. This facilitates the identification of regions of non-ideal charge extraction in the solar cells and enables to link these to the processing conditions. The proposed technique highlights that, combined with potentiostatic measurements, luminescence microscopy turns out to be a powerful tool for the assessment of performance losses and the improvement of solar cells.

Introduction

The current density - voltage ($J(V)$) curve builds the basis of any further characterization and improvement of solar cells and other opto-electronic devices. This characteristic provides a broad range of information on the fundamental mechanisms such as charge carrier generation, recombination, and transport losses. Conventionally, the $J(V)$-curve is measured by illuminating the full device and externally probing the current flowing between the electrodes with a source meter. This approach therefore only provides information integrated over the entire device area. A range of techniques have been established for spatially resolved analysis of photovoltaic devices[1,2] such as light beam induced current mapping (LBIC),[3–5] lock-in thermography (LIT),[6–8] photoluminescence (PL) imaging,[3,9–23] and electroluminescence (EL) imaging.[24] However, as further discussed in the Supporting Information (SI), these techniques can either probe only a portion of the local $J(V)$ characteristic or require numerical fitting to a postulated diode model. Especially for emerging PV technologies like perovskite solar cells (PSC) it is crucial to gain spatially resolved fundamental information about the charge transport and the extraction phenomena on microscopic as well as on macroscopic scale to further enhance the power conversion efficiency and long-term stability of these cells. Therefore, novel advanced characterization techniques are necessary.

The physics of optoelectronic devices can be divided into fundamental operation processes. For photovoltaic power generation, these are the photo-generation of charge carriers by the absorption of photons, the transport to and separation of the photogenerated electrons and holes at charge extraction layers (CELs), and the extraction of the charges into the outer device terminals (cables). The three processes have been described by so-called reciprocity relations by Donolato,[25] Rau,[26] and Wong and Green,[27] respectively. To each of these processes, fundamental loss mechanisms can be assigned, namely optical and absorption losses, radiative and non-radiative recombination mechanisms, and transport losses.

In this work, we introduce a method based on electrical bias dependent photoluminescence imaging that allows the immediate determination of the charge extraction efficiency of photo-generated charge carriers. The approach makes use of the observation that the difference of two photoluminescence images at different bias voltages yields direct spatially resolved information on the local $J(V)$. We propose to refer to this method as local charge extraction analysis by “Potentiostatic Photoluminescence Imaging” (PPI). We outline the theoretical principles of the PPI approach and experimentally demonstrate the validity by means of a close-to-ideal GaInAsP solar cell. The potential to identify morphological features of benign and poor charge extractions are investigated by means of high-efficiency (>20 %) perovskite solar cell investigating both microscopic images of the local short-circuit current J_{sc} in steady state as well as local $J(V)$ curves. Based on these results, we demonstrate how distinct charge extraction signatures of the PPI method can be linked to physical properties of the perovskite layer, the charge extraction layers, and the respective interfaces.

Theory

The PPI method is based on a detailed balance approach, considering that in steady state, the current density measured at the outer solar cell contacts, $J(V)$, can be expressed by the current density of the photo-generated charge carriers, J_{gen}, and the (internal) recombination in the perovskite layer and at respective interfaces, $J_{rec}(V)$,

$$J(V) = J_{gen} - J_{rec}(V) . \qquad (1)$$

Here, we assume that in the considered operation range ($0\ V \leq V \leq V_{oc}$), the internal generation current J_{gen} is not affected by the applied bias. Moreover, without loss of generality, we assume that the photon flux to illuminate the sample is constant over time and spatially homogeneous.

The internal recombination processes comprise non-radiative and radiative components, $J_{n.r.}$ and J_{rad}, respectively: $J_{rec} = J_{n.r.} + J_{rad}$. They can be related to each other by

$$J_{n.r.}(V) = k(V) \cdot J_{rad}(V) . \qquad (2)$$

Equation (2) is generally valid if k is a function of the applied bias, $k = k(V)$. Here, we show that, if the probed sample has a diode ideality factor close to one and displays negligible resistive losses (high shunt resistance, low series resistance), then it is justified to assume a linear relationship between $J_{n.r.}(V)$ and $J_{rad}(V)$ and hence k = const., which we will assume in the following. Empirical indications for this circumstance in perovskite solar cells have already been presented by Stolterfoht and coworkers.[23] A detailed theoretical discussion of this assumption as well as a general expression are presented in the Supporting Information (SI section B).

Now, Equation (1) can be expressed as

$$J(V) = J_{gen} - (1 + k) \cdot J_{rad}(V). \quad (3)$$

$J_{rad}(V)$ can be related to the signal of a photodetector $S_{PL}(V)$ by

$$S_{PL}(V) = c \frac{J_{rad}(V)}{e}, \quad (4)$$

where c describes the probability that photons created by radiative recombination enter the detector area and are translated into a detector signal.

Using Equation (3), and (4), we can now relate the electrical photocurrent to the difference between the voltage-dependent PL intensity PL(V) and the PL at open circuit. By normalizing the term, the expression becomes independent of setup-specific factors which makes the technique independent from elaborate calibration measures. We find that

$$\frac{S_{PL}(V_{oc}) - S_{PL}(V)}{S_{PL}(V_{oc})} = \frac{J(V)}{J_{gen}}. \quad (5)$$

This relation shows that photoluminescence microscopy can be used to derive spatially as well as time-resolved images of the local $J(V)$ performance of a photovoltaic device. Two applications are especially interesting: First, by recording only two PL images, one at open circuit and one at short circuit, the image of the local short-circuit photocurrent density J_{sc} can be derived. Secondly, by recording PL images at various voltages, the local $J(V)$ of specific spots on the cell can be investigated. These approaches are investigated in the following. Thereby, the $J(V)/J_{gen}$ results determined by PL microscopy will be denoted as $J(V)/J_{gen}|_{PL}$.

Results And Discussion

Experimental validation of the PPI approach

III-V-based photovoltaic device

Many III-V compound semiconductors, such as gallium-arsenide (GaAs), indium-phosphide (InP), or combinations like $Ga_xIn_{1-x}As_yP_{1-y}$, have a direct band gap. Hence, for III-V semiconductor crystals with a low defect density radiative recombination is the dominant recombination mechanism. In addition, the high absorption coefficient allows using thin absorber layers in the order of a few micrometers. This fact along with sufficiently high carrier mobilities and lifetimes promises high power conversion potential of this material class in photovoltaic applications.[28,29] III-V compound semiconductors can be grown epitaxially with high crystal quality using for instance metalorganic vapor phase epitaxy (MOVPE). The

highest efficiencies of both single- and multi-junction solar cells under the AM1.5g solar spectrum and under concentration were achieved with III-V based devices, reaching efficiencies as high as 47.1 %.[30–32]

To test the assumptions made in Equation (3), a $Ga_{0.91}In_{0.09}As_{0.83}P_{0.17}$ solar cell with almost ideal photovoltaic properties in terms of diode behavior and transport losses as derived from a one-diode model fit to a measured current-voltage characteristic was studied (cf. SI). Figure 1 displays the current voltage characteristic of this III-V semiconductor device and the simultaneously recorded PL(V) curve. The remarkable overlap of these measurements highlights the validity of the above outlined theoretical considerations. .

By applying a baseline correction considering the reflectance of the sample, at short circuit ($J(0) = J_{sc}$), the charge extraction efficiency $J_{sc}/J_{gen}|_{PL}$ is assessed to be 0.87 from the PPI measurements. To validate this result, as the internal quantum efficiency (IQE) was determined by a direct measurement of the external quantum efficiency (EQE) and the reflectance of the device at a wavelength of 620 nm, close to the excitation wavelength of the PPI setup of 623 nm. The IQE value of 0.98 (cf. SI) is in good agreement to $J_{sc}/J_{gen}|_{PL}$. The remaining difference of around 10 % can likely be attributed to the propagation of measurement uncertainties from all the methods that were involved.

Perovskite-based photovoltaic device

Monocrystalline, wafer-based PV devices like III-V solar cells display very homogeneous photoluminescence features (cf. Figure S5). To assess the full potential of microscopically resolved charge extraction imaging by the PPI approach, measurements were carried out on a high-efficiency perovskite solar cell with a layer structure of glass / fluorine-doped tin oxide (FTO) / compact titanium dioxide (TiO_2) / mesoporous TiO_2 / perovskite / Spiro-OMeTAD / Au. Stabilized measurements of the *J-V* parameters under AM 1.5g illumination yielded a stabilized PCE of 21.2 %, a stabilized J_{sc} of 26.4 mA/cm², and a stabilized V_{oc} of 1.03 V (cf. Figure S4 in the SI).

Despite the high performance, the microscopic PL-image of the device recorded at open circuit conditions (PL(V_{oc})) shown in Figure 2a displays a highly inhomogeneous pattern of the active area. The image reveals morphological patterns that are typically assigned to perovskite films formed by spin coating such as stripes and dots. In the region of highest PL(V_{oc}) such as spot (i), the PL intensity exceeds that of the surrounding area by more than a factor of five. Figure 2b displays the image of the local short circuit current assessed by PPI measurements in steady state, i.e., after stabilizing the devices for longer than 60 s. As can be seen in the $J_{sc}/J_{gen}|_{PL}$ image, it can be misleading to directly conclude from the PL(V_{oc}) image on the local device performance. In the $J_{sc}/J_{gen}|_{PL}$ representation, the active area is relatively more homogeneous and will reveal more meaningful information on the aforementioned morphological patterns. Concerning regions of high PL(V_{oc}), the PPI method allows to distinguish between two distinct features: feature (i) displays a spot with very low $J_{sc}/J_{gen}|_{PL}$, i.e., the PL intensity is not quenched when switching from open to short circuit. While the high PL(V_{oc}) is a clear indicator for the presence of high-quality perovskite crystals with low non-radiative recombination, the low $J_{sc}/J_{gen}|_{PL}$ suggests a poor

electrical connection of the perovskite to the charge extraction layers. In contrast, feature (ii) displays both high PL(V_{oc}) and high J_{sc}/J_{gen} $|_{PL}$, due to a benign electrical coupling. A detailed discussion on experimental limitations of the approach and calibration strategies is presented in the SI.

J (V) imaging

Figure 3a shows the microscopic PL(V_{oc}) image of another perovskite solar cell, displaying similar patterns as the sample discussed above. The patterns were grouped according to the pattern type and PL intensity in the PL(V_{oc}) image: dots (A) and stripe patterns (B) with lower PL(V_{oc}) as well as stripes with higher PL(V_{oc}) (C) (cf. magnified image in Figure 3b). With the PPI method, we can retrieve the local $J(V)/J_{gen}$ $|_{PL}$ curve for each pixel of the microscope image. Figure 3c shows the corresponding $J(V)/J_{gen}$ $|_{PL}$ curve for the features A, B, and C. One can see that the similarities from the PL(V_{oc}) images are also found in the $J(V)/J_{gen}$ $|_{PL}$ representation, where the J_{sc} is highest for features C, lower for B and lowest for A. This demonstrates the potential to directly record the local $J(V)/J_{gen}$ $|_{PL}$ image with microscopic resolution.

At this point, it is important to note that the method implicitly assumes that the V_{oc} is equal over the entire cell area. This assumption is only valid if the absorber is well coupled to the outer electrodes and if the sheet resistivity of the electrodes is low. Finally, it is important to take the unique transient behavior of perovskite material into account for any luminescence measurement.[24] For PSC, reaching a stabilized state after changes in electrical bias, illumination, or even atmospheric conditions can require minutes to hours.[33–35] Moreover, non-reversible degradation processes can take place in these timeframes and under these conditions.[36,37] A discussion of the transient behavior can be found in the SI.

The influence of interfaces on charge extraction

To investigate the effect of the different PSC layers on local extraction of photogenerated charge carriers, a range of spin-coated perovskite cells with an n-i-p structure were studied for which the optimal layer configuration of glass / TCO / electron-extraction layer / perovskite / hole-extraction layer / Au was intentionally altered. Figure 4 shows the microscopic images of PL(V_{oc}) and J_{sc}/J_{gen} $|_{PL}$, respectively, for a solar cell with reduced perovskite layer thickness (a, b), a device without electron- extraction layer (EEL) (c, d), and one without hole-extraction layer (HEL) (e, f). The J_{sc}/J_{gen} $|_{PL}$ averaged over the entire image is 0.71, 0.24, and 0.11, respectively.

The images reveal a range of interesting features and general observations: in Figure 4a and b, stripe or wave patterns can be recognized that are most probably caused by the spin-coating process. For these patterns, high PL(V_{oc}) correlates with high J_{sc}/J_{gen} $|_{PL}$. Comparing the two images furthermore demonstrates that by only employing the PL(V_{oc}), some features remain concealed which become visible in the J_{sc}/J_{gen} $|_{PL}$-representation. In this sense, features (iii) and (iv) in the bottom of the image are most striking for which the low J_{sc}/J_{gen} $|_{PL}$ indicates poor charge extraction. In feature (iii), also the PL(V_{oc}) is low, indicating that the perovskite is severely degraded (or absent) at this spot. In contrast, for feature (iv),

the PL(V_{oc}) in the same range as for the surroundings which shows that photovoltaic active material is present here. However, the $J_{sc}/J_{gen}|_{PL}$ image reveals that the photogenerated charges are not extracted.

Looking at the EEL-free devices in Figure 4c and d, we observe an absence of the wave pattern. Hence, this pattern is most probably induced by the spin-coating process of the EEL. Two additional features appear here. Similar to spot (v), feature (vi) has a high PL(V_{oc}) but a low $J_{sc}/J_{gen}|_{PL}$. Inversely, there are many small spots, as represented by three circles for features (iv) that are prominent due to a high $J_{sc}/J_{gen}|_{PL}$. In the PL(V_{oc}) image, they can, however, not be distinguished from the surrounding regions.

The HEL-free devices again do show the wave-pattern (Figure 4e, f). The PL(V_{oc}) is much lower than for the other samples (note that the color scale was divided by a factor of 10). Also, the $J_{sc}/J_{gen}|_{PL}$ is low throughout most of the observed area. There are a few small dots as represented by feature (v) that display both relatively high PL(V_{oc}) and high $J_{sc}/J_{gen}|_{PL}$. In contrast, similar to features (iii) and (iv), feature (viii) shows high PL(V_{oc}) but low $J_{sc}/J_{gen}|_{PL}$.

Further assessments of the effect of the metal back electrode and a comparison of *I-V* parameters with PL data can be found in the SI.

Identification of charge extraction loss mechanisms

The measurements presented above demonstrate that the $J(V)/J_{gen}|_{PL}$ approach is a simple and powerful tool to analyze the local performance of perovskite solar cells with microscopic resolution. As the $J_{sc}/J_{gen}|_{PL}$ representation also contains information on the local PL(V_{oc}) and PL(V=0), we can use this method to unravel interfacial charge extraction and recombination mechanisms that would not be possible using methods like LBIC alone. This means that we are not only able to detect regions of low photocurrent but can also estimate why the current is low. Such an investigation is especially significant for the characterization of solution-processed solar cells like PSC where a key challenge is the establishment of good electrical coupling between the perovskite crystals and the charge extraction layers.[38]

Figure 5a illustrates how $J_{sc}/J_{gen}|_{PL}$ can be span by the corresponding PL(V_{oc}) and PL(V=0) intensities. A high $J_{sc}/J_{gen}|_{PL}$ is achieved if PL is high at open circuit and zero at short circuit. On this map, we can now classify features of the above studied samples within a set of extreme cases.

1. In the **ideal case**, $J_{sc}/J_{gen}|_{PL}$ approaches unity. This means that the non-radiative recombination is minimized, and radiative recombination is maximized. Practically, this situation is reached if there is full coverage of a high-quality perovskite crystal layer (corresponding to a maximal PL(V_{oc}) at open circuit), while the photogenerated charge carriers are ideally extracted at short circuit. This is represented by the white area at the ordinate of the graph in Figure 5a and by situation (1) in Figure 5b where a schematic cross-section of a PSC is displayed. Features (ii), (vi), and (vii) approach this ideal situation.

A $J_{sc}/J_{gen}|_{PL}$ of zero occurs for two worst-case scenarios:

2. There is **no presence of a functional perovskite layer**, as for the case of degraded perovskite or even complete absence of this layer, as depicted by situation (2) Figure 5b. This situation can be identified if PL(V_{oc}) is also zero, as represented by the origin in the graph of Figure 5a). Such a situation can be attributed to feature (iii)
3. A perovskite layer is present, but there is **no efficient charge extraction** of the photogenerated charge carriers to the outer terminals. In the most dramatic case, this occurs in the absence of a back electrode, as illustrated by case (3) in Figure 5b. In this case, the PL is not changed at short circuit and thus PL(V_{oc}) = PL(V=0), represented by the black area at the bisector in Figure 5a. Due to a lower surface recombination, in practice the PL(V_{oc}) is likely higher in these regions in comparison to those with good connection to contact layers. Features (v) and (viii) are representative for this situation.
4. Finally, there is also the possibility of **poor charge selectivity**. This can be the case for an absence of charge selective layers such that the back or front electrode is directly in contact with the perovskite absorber (case (4, 4') in Figure 5b). Another possibility is a high surface recombination/ poor selectivity of the EEL or HEL. In this case, the PL(V=0) can be zero, but due to high surface recombination, PL(V_{oc}) is also low. The entire active area of the devices without EEL or HEL displayed in Figure 4d and f are representative for this situation.

Conclusion

The photocurrent-voltage ($J(V)$) curve is the key characteristic for assessing photovoltaic devices. However, $J(V)$ measurements usually do not contain any spatial information, which are essential for a deeper understanding and further improvements of the devices. A range of methods for the local assessment of the photocurrent have been developed, especially for silicon and III-V solar cells. Yet, none of them has so far been able to offer a combination of the possibility to assess the local $J(V)$ for all bias voltages between 0 V and V_{oc} while at the same time yielding fast image acquisition at microscopical resolution.

With the PPI approach, we introduced a straightforward method for a time-resolved assessment of the local photovoltaic $J(V)$ curve of perovskite solar cells by electrical-bias dependent luminescence microscopic imaging. We derived from basic principles how the measurement of the difference in PL(V) to the PL(V_{oc}) at open circuit can be related to the local $J(V)$. The validity of the approach was experimentally demonstrated by applying it to a close-to-ideal III-V solar cell. Challenges and opportunities of the approach were systematically studied and discussed. By the investigation of a high performing (>20 %) perovskite solar cell, we showed that the PPI approach allows the real-time assessment of the microscopically resolved local assessment of the $J(V)$ curve, the steady-state J_{sc} as well as transient charge extraction behavior. Furthermore, we demonstrated that the technique also reveals information to assess the local charge extraction efficiency and interfacial recombination mechanisms. It is therefore a valuable tool for the understanding of the electrical coupling of the perovskite to the charge extraction layers. This work shows that, combined with potentiostatic measurements, microscopic luminescence imaging can be a powerful tool for the assessment of

performance losses and the improvement of solar cells. The introduced technique can make a significant impact on the understanding and improvement of perovskite and other solar cell technologies as it enables relating morphological artifacts to device performance at a microscopic resolution.

Methods

The photoluminescence intensity was measured in reflectance with an optical microscope at 10x magnification. A red and blue high-power LED (Thorlabs Solis) with a peak intensity of 632 and 405 nm, respectively, was used to illuminate the solar cells at a light intensity equivalent to one sun as determined by measuring a reference silicon PV cell and calculating the photon flux from the EQE spectrum. On the detector side, the PL light was focussed onto a high resolution sCMOS camera (Andor Zyla 5.5) with an optical high-pass filter (cut-off at 760 nm). To apply an electrical bias and to simultaneously measure solar cell currents and voltages, a potentiostat (Ivium CompactStat) was used. After changing the electrical bias, the PL was stabilized for at least 60 seconds before recording the image of perovskite devices.

Stabilized current-voltage parameters such as PCE, J_{sc} and V_{oc} were determined by under a class A solar simulator whose intensity was calibrated with a silicon reference cell, where for perovskite devices ‘stabilized’ refers to the value measured after 100 s of measurement. For the determination of the stabilized PCE, the device current was recorded under a fixed bias voltage close to the suspected maximum power point.

Processing parameters of solar cells are outlined in the SI.

Declarations

Acknowledgements

L.W., J.P.H., S.M., and U.W. acknowledge the funding from the European Union’s Horizon 2020 research and innovation program under Grant Agreement No.763989 (APOLO). This publication reflects only the author’s views and the European Union is not liable for any use that may be made of the information contained therein. L.W., M.E., D.B., S.Z., S.M. and A.H. acknowledge funding within the project UNIQUE, supported under the umbrella of SOLAR-ERA.NET_Cofund by ANR, PtJ, MIUR, MINECOAEI, SWEA. SOLAR-ERA.NET is supported by the European Commission within the EU Framework Programme for Research and Innovation HORIZON 2020 (Cofund ERANET Action, No. 691664). L.W. and D.B. acknowledge scholarship support by the German Federal Environmental Foundation (DBU). P. S. acknowledges his PhD scholarship from the Heinrich-Böll Foundation. S.Z. acknowledges scholarship support by the German Academic Exchange Service (DAAD). We thank Markus Glatthaar (Fraunhofer ISE) for valuable discussions.

Author contributions

L.W. and A.H. developed the idea of the PPI approach, derived the theory and conceived the initial measurement. The concept was intensively discussed and the measurement method was refined by the significant contribution of L.W., J.P.H., P.S., M.E., D.B., S.Z., S.M. U.W., A.H. and S.G.. L.W. wrote the manuscript, developed, and carried out PPI measurements and data analysis on III-V devices together with P.S. and on PSC, together with J.P.H., M.E., D.B., and S.Z. Perovskite samples were provided by and data on PSC was discussed with at Y.L, S.M.Z, and M.G.. III-V samples were fabricated and further characterized by P.S. All authors discussed the results and revised the manuscript

References

1. Schubert, M. C., Mundt, L. E., Walter, D., Fell, A. & Glunz, S. W. Spatially Resolved Performance Analysis for Perovskite Solar Cells. *Adv. Energy Mater.*, 1904001; 10.1002/aenm.201904001 (2020).
2. Fertig, F. *et al.* Short-circuit Current Density Imaging Methods for Silicon Solar Cells. *Energy Procedia* **77**, 43–56; 10.1016/j.egypro.2015.07.008 (2015).
3. Mundt, L. E. *et al.* Quantitative Local Loss Analysis of Blade-Coated Perovskite Solar Cells. *IEEE Journal of Photovoltaics*, 1–8; 10.1109/JPHOTOV.2018.2888835 (2019).
4. Seager, C. H. The determination of grain-boundary recombination rates by scanned spot excitation methods. *J Appl Phys* **53**, 5968–5971; 10.1063/1.331389 (1982).
5. Padilla, M., Michl, B., Thaidigsmann, B., Warta, W. & Schubert, M. C. Short-circuit current density mapping for solar cells. *Solar Energy Materials and Solar Cells* **120**, 282–288; 10.1016/j.solmat.2013.09.019 (2014).
6. Fertig, F., Greulich, J. & Rein, S. Spatially resolved determination of the short-circuit current density of silicon solar cells via lock-in thermography. *Appl Phys Lett* **104**, 201111; 10.1063/1.4876926 (2014).
7. Breitenstein, O., Fertig, F. & Bauer, J. An empirical method for imaging the short circuit current density in silicon solar cells based on dark lock-in thermography. *Photovoltaics, Solar Energy Materials, and Technologies: Cancun* 2010 **143**, 406–410; 10.1016/j.solmat.2015.07.027 (2015).
8. Breitenstein, O. Nondestructive local analysis of current–voltage characteristics of solar cells by lock-in thermography. *Solar Energy Materials & Solar Cells* **95**, 2933–2936; 10.1016/j.solmat.2011.05.049 (2011).
9. Rietwyk, K. J. *et al.* Light intensity modulated photoluminescence for rapid series resistance mapping of perovskite solar cells. *Nano Energy* **73**, 104755; 10.1016/j.nanoen.2020.104755 (2020).
10. Walter, D. *et al.* On the Use of Luminescence Intensity Images for Quantified Characterization of Perovskite Solar Cells. Spatial Distribution of Series Resistance. *Adv. Energy Mater.* **5**, 1701522; 10.1002/aenm.201701522 (2017).

11. Mundt, L. E. *et al.* Nondestructive Probing of Perovskite Silicon Tandem Solar Cells Using Multiwavelength Photoluminescence Mapping. *IEEE Journal of Photovoltaics* **7**, 1081–1086; 10.1109/JPHOTOV.2017.2688022 (2017).
12. Soufiani, A. M. *et al.* Lessons Learnt from Spatially Resolved Electro- and Photoluminescence Imaging. Interfacial Delamination in CH 3 NH 3 PbI 3 Planar Perovskite Solar Cells upon Illumination. *Advanced Energy Materials* **49**, 1602111; 10.1002/aenm.201602111 (2016).
13. Okano, M. *et al.* Degradation mechanism of perovskite CH 3 NH 3 PbI 3 diode devices studied by electroluminescence and photoluminescence imaging spectroscopy. *Appl Phys Express* **8**, 102302; 10.7567/APEX.8.102302 (2015).
14. Hameiri, Z. *et al.* Photoluminescence and electroluminescence imaging of perovskite solar cells. *Progress in Photovoltaics* **23**, 1697–1705; 10.1002/pip.2716 (2015).
15. Mastroianni, S. *et al.* Analysing the effect of crystal size and structure in highly efficient CH3NH3PbI3 perovskite solar cells by spatially resolved photo- and electroluminescence imaging. *Nanoscale* **7**, 19653–19662; 10.1039/C5NR05308K (2015).
16. Hoffler, H., Breitenstein, O. & Haunschild, J. Short-Circuit Current Density Imaging Via PL Image Evaluation Based on Implied Voltage Distribution. *IEEE J. Photovolt.* **5**, 613–618; 10.1109/JPHOTOV.2014.2379097 (2015).
17. Haunschild, J., Glatthaar, M., Kasemann, M., Rein, S. & Weber, E. R. Fast series resistance imaging for silicon solar cells using electroluminescence. *Physica Status Solidi RRL* **3**, 227–229; 10.1002/pssr.200903175 (2009).
18. Breitenstein, O., Höffler, H. & Haunschild, J. Photoluminescence image evaluation of solar cells based on implied voltage distribution. *Photovoltaics, Solar Energy Materials, and Technologies: Cancun 2010* **128**, 296–299; 10.1016/j.solmat.2014.05.040 (2014).
19. Glatthaar, M. *et al.* Spatially resolved determination of dark saturation current and series resistance of silicon solar cells. *physica status solidi (RRL) - Rapid Research Letters* **4**, 13–15; 10.1002/pssr.200903290 (2010).
20. Glatthaar, M. *et al.* Evaluating luminescence based voltage images of silicon solar cells. *J Appl Phys* **108**, 14501; 10.1063/1.3443438 (2010).
21. Kampwerth, H., Trupke, T., Weber, J. W. & Augarten, Y. Advanced luminescence based effective series resistance imaging of silicon solar cells. *Applied Physics Letters* **93**, 202102; 10.1063/1.2982588 (2008).
22. Trupke, T., Pink, E., Bardos, R. A. & Abbott, M. D. Spatially resolved series resistance of silicon solar cells obtained from luminescence imaging. *Appl Phys Lett* **90**, 93506; 10.1063/1.2709630 (2007).
23. Stolterfoht, M. *et al.* Voltage-Dependent Photoluminescence and How It Correlates with the Fill Factor and Open-Circuit Voltage in Perovskite Solar Cells. *ACS Energy Lett.* **4**, 2887–2892; 10.1021/acsenergylett.9b02262 (2019).
24. Soufiani, A. M., Kim, J., Ho-Baillie, A., Green, M. & Hameiri, Z. Luminescence Imaging Characterization of Perovskite Solar Cells: A Note on the Analysis and Reporting the Results. *Adv. Energy Mater.* **8**,

1702256; 10.1002/aenm.201702256 (2018).

25. Donolato, C. A reciprocity theorem for charge collection. *Ultramicroscopy* **46**, 270–272; 10.1063/1.95654 (1985).
26. Rau, U. Reciprocity relation between photovoltaic quantum efficiency and electroluminescent emission of solar cells. *Thin Solid Films* **76**, 435; 10.1103/PhysRevB.76.085303 (2007).
27. Wong, J. & Green, M. From junction to terminal: Extended reciprocity relations in solar cell operation. *Phys Rev B* **85**; 10.1103/PhysRevB.85.235205 (2012).
28. Rau, U., Blank, B., Müller, T. C. M. & Kirchartz, T. Efficiency Potential of Photovoltaic Materials and Devices Unveiled by Detailed-Balance Analysis. *Phys. Rev. Applied* **7**; 10.1103/PhysRevApplied.7.044016 (2017).
29. Kirchartz, T. & Rau, U. What Makes a Good Solar Cell? *Adv. Energy Mater.* **8**, 1703385; 10.1002/aenm.201703385 (2018).
30. Green, M. *et al.* Solar cell efficiency tables (version 57). *Prog Photovoltaics* **29**, 3–15; 10.1002/pip.3371 (2021).
31. Kayes, B. M. *et al.* 27.6% conversion efficiency, a new record for single-junction solar cells under 1 sun illumination. In *Conference Record of the 37th IEEE Photovoltaic Specialists Conference* (IEEE, Piscataway, NJ, Piscataway, NJ, 2011), pp. 4–8.
32. Geisz, J. F. *et al.* Six-junction III–V solar cells with 47.1% conversion efficiency under 143 Suns concentration. *Nat Energy* **5**, 326–335; 10.1038/s41560-020-0598-5 (2020).
33. Xu, Z., Rosia, T. de & Weeks, K. Photoluminescence–Voltage (PL– V) Hysteresis of Perovskite Solar Cells. *J Phys Chem C* **121**, 24389–24396; 10.1021/acs.jpcc.7b06711 (2017).
34. Chen, S. *et al.* Light Illumination Induced Photoluminescence Enhancement and Quenching in Lead Halide Perovskite. *Sol. RRL* **1**, 1600001; 10.1002/solr.201600001 (2017).
35. Howard, J. M. *et al.* Humidity-Induced Photoluminescence Hysteresis in Variable Cs/Br Ratio Hybrid Perovskites. *J. Phys. Chem. Lett.* **9**, 3463–3469; 10.1021/acs.jpclett.8b01357 (2018).
36. Khenkin, M. V. *et al.* Dynamics of Photoinduced Degradation of Perovskite Photovoltaics: From Reversible to Irreversible Processes. *ACS Appl. Energy Mater.* **1**, 799–806; 10.1021/acsaem.7b00256 (2018).
37. Gomez, A., Sanchez, S., Campoy-Quiles, M. & Abate, A. Topological distribution of reversible and non-reversible degradation in perovskite solar cells. *Nano Energy* **45**, 94–100; 10.1016/j.nanoen.2017.12.040 (2018).
38. Wagner, L. *et al.* Distinguishing crystallization stages and their influence on quantum efficiency during perovskite solar cell formation in real-time. *Sci. Rep.* **7**, 14899; 10.1038/s41598-017-13855-6 (2017).

Figures

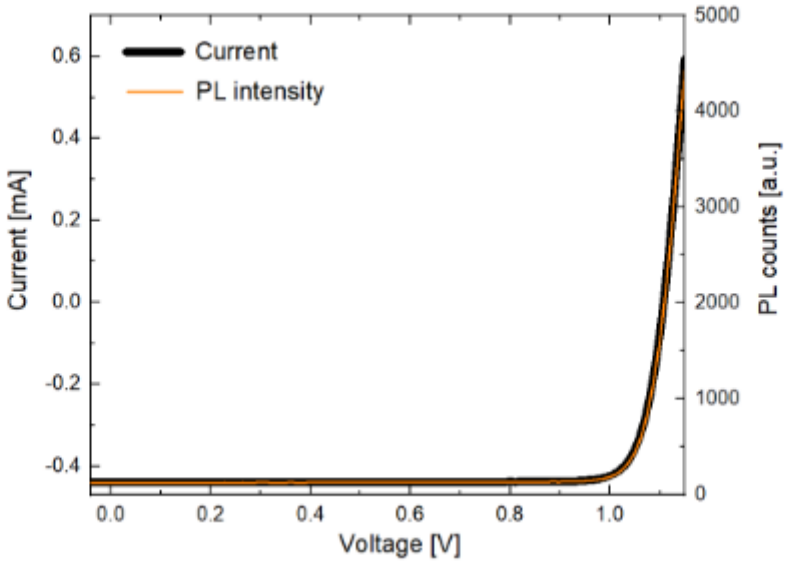

Figure 1

Current-voltage characteristic of a highly efficient (18.7 % power conversion efficiency) Ga0.91In0.09As0.83P0.17 solar cell (thick black line), compared with the simultaneously recorded PL(V) characteristic (thin orange line).

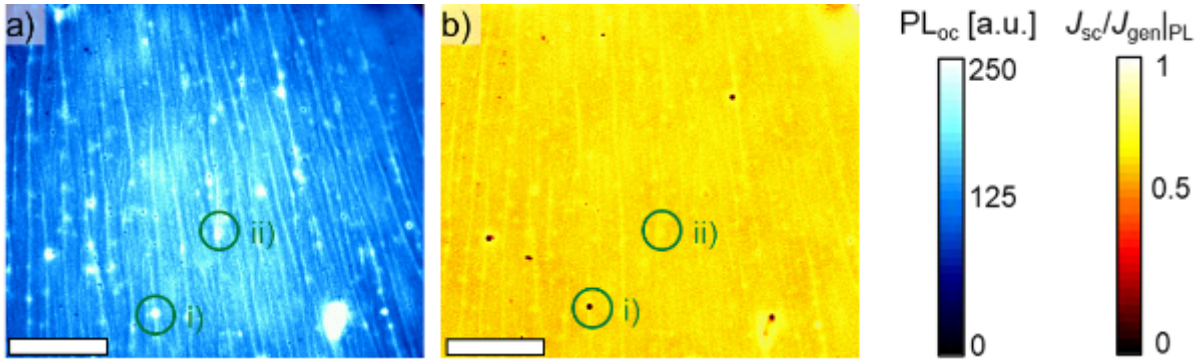

Figure 2

a) PL(Voc) and (b) Jsc/Jgen |PL determined from two PL images at open and short circuit of a high performing (>20%) perovskite solar cell. The device was illuminated with a red LED (632 nm). The scale bar corresponds to 400 µm in both images.

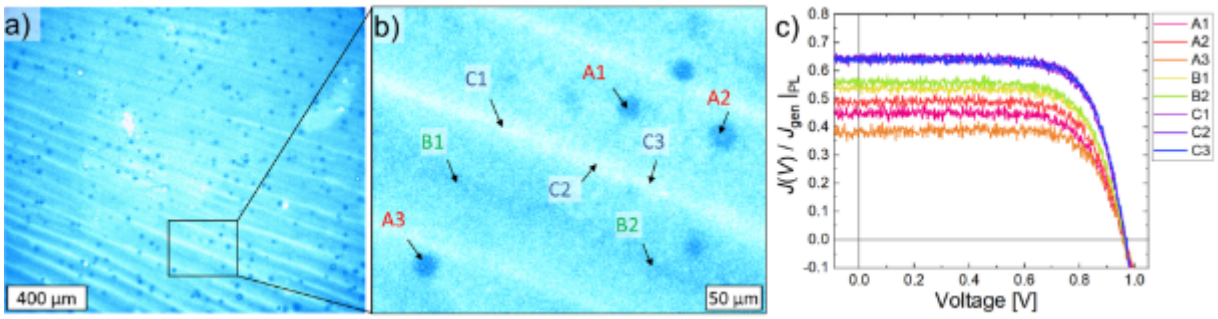

Figure 3

a) PL(Voc) intensity map of a sample in open circuit and b) closeup of a selected area. c) Local J(V)/Jgen |PL curve of the spots highlighted in (b) for a slow reverse voltage scan (20 mV/s). The sample was illuminated with a 632 nm LED light.

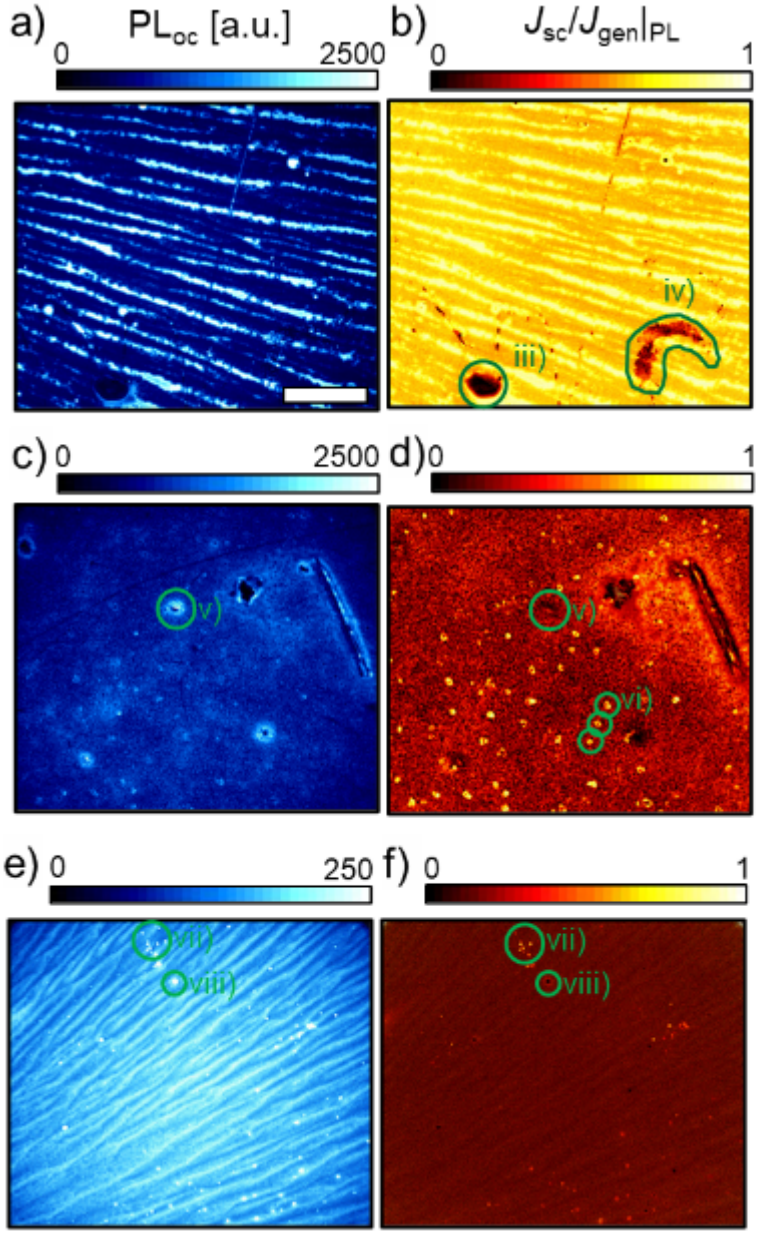

Figure 4

PL at open circuit (PL(Voc), blue images) and normalized short circuit photocurrent density (Jsc/Jgen |PL, red images) imaging analysis. Three different spin-coated n-i-p PSC are shown, respectively: A cell with reduced perovskite layer thickness (a, b) as well as an EEL-layer free (c, d) and an HEL-layer free device (e, f). Note that the PL(Voc) intensity of images a) and c) ranges up to 2500 counts whereas image e) ranges only up to 250 counts. The samples were illuminated with a 632 nm LED light. The scale bar represents 400 µm for all images.

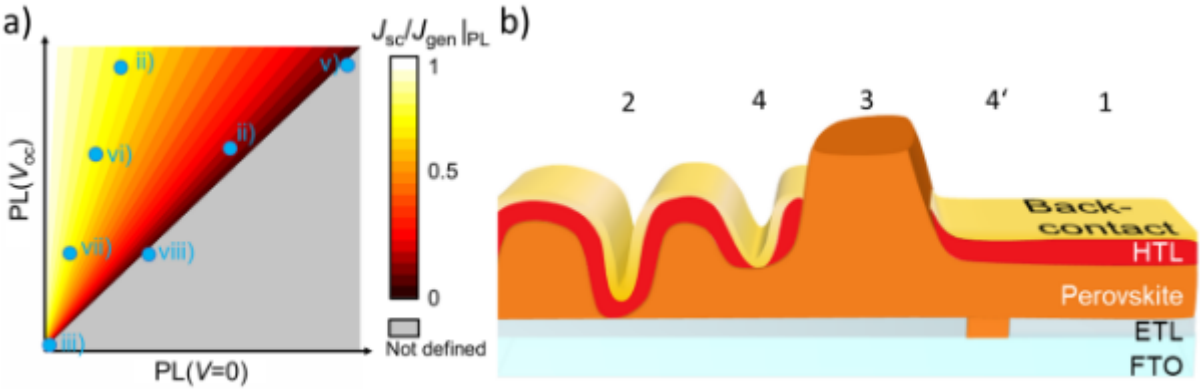

Figure 5

a) Evolution of the charge extraction coefficient respective to short circuit, Jsc/Jgen |PL, for different values of PL intensity at open and short circuit. The blue dots correspond the features from Figures 2 and 4. b) Schematic illustration of the cross section of a n-i-p perovskite solar cell, displaying four characteristic cases for (non) ideal charge extraction.

Supplementary Files

This is a list of supplementary files associated with this preprint. Click to download.

- 211018PPINatComSI.pdf